Friction **9**(5): 929–940 (2021)
https://doi.org/10.1007/s40544-020-0376-1
ISSN 2223-7690
CN 10-1237/TH
RESEARCH ARTICLE

Tribocorrosion properties of AISI 1045 and AISI 2205 steels in seawater: Synergistic interactions of wear and corrosion

Beibei ZHANG[1], Jianzhang WANG[1], Hao LIU[1], Yunfeng YAN[1,2], Pengfei JIANG[1], Fengyuan YAN[1,*]

[1] *State Key Laboratory of Solid Lubrication, Lanzhou Institute of Chemical Physics, Chinese Academy of Sciences, Lanzhou 730000, China*

[2] *Center of Materials Science and Optoelectronics Engineering, University of Chinese Academy of Sciences, Beijing 100049, China*

Received: 08 May 2019 / Revised: 19 October 2019 / Accepted: 24 February 2020

Abstract: Tribocorrosion denotes an irreversible material degradation for several metallic components used in corrosive environments, and it arises from the interplay between chemical, mechanical, and electrochemical processes. In this study, some investigation has been performed to compare the tribocorrosion behavior of AISI 1045 steel and AISI 2205 duplex stainless steel sliding against an alumina pin in seawater. The lowering in the open circuit potential (OCP) of AISI 2205 during the tribocorrosion demonstrates that its protective passive film was damaged by wear and resulted in a wear-accelerated corrosion in the wear track. However, sliding was found to accelerate the corrosion of the unworn areas for AISI 1045, leading to an anodic shift of the OCP. Moreover, the total material loss increased with an increase in the applied potential for both materials. It was revealed that AISI 1045 was more sensitive to corrosion under sliding than AISI 2205. Therefore, pure corrosion loss and corrosion-induced wear constituted the primary reasons for the degradation of AISI 1045 at applied anodic potentials.

Keywords: tribocorrosion; passivation; synergistic effect; seawater

1 Introduction

Metallic materials are extensively used in corrosive environments owing to their ability to form protective passive film. However, in the practical engineering applications, e.g., stern tube bearings and offshore platforms, these passive metals often undergo tribological contacts, which will damage or even remove their protective oxide film exposing the underlying fresh bulk material to the surrounding corrosive environment [1–4]. Therefore, the metals are subjected to accelerated material loss through a combined influence of mechanical and electrochemical damage. Owing to the coupling of mechanical loading and corrosive attack by the environment, this tribocorrosion behavior of material might not be predicted separately based on wear or corrosion. This indicates that the total material loss caused by tribocorrosion is often significantly higher than the degradation by the individual processes. Therefore, the synergistic effect between wear and corrosion usually plays an important role in material failure, which poses a high potential safety risk and generates huge economic losses [5–7].

The use of stainless steels is prevailing in harsh environments owing to its good mechanical properties and high corrosion resistance. It is generally acknowledged that these alloys derive their corrosion resistance from the generation of a chromium passive film on the surface [8–12]. All stainless steel are

* Corresponding author: Fengyuan YAN, E-mail: fyyan@licp.cas.cn

iron-based alloys that contain enough chromium and nickel, which can be divided into four grades, namely austenitic, martensitic, ferritic, and duplex stainless steel. Especially, duplex stainless steel exhibits excellent properties as it is composed of a mixed austenite/ferrite dual-phase microstructure allowing it to display the combined properties of both phases. In many situations, duplex stainless steels are employed in corrosive environment coupled with wear actions, such as sliding bearings and sealing surfaces in chloride-containing environment, where unexpected damage can be observed due to the synergistic effects between wear and corrosion [13–15]. It is further emphasized that the breakdown of passive film might considerably change the overall behavior of duplex stainless steels under tribological contacts, e.g., by initiating the galvanic corrosion. The carbon steels, which are used in a wide range of applications, such as structural components, shafting, industrial pipeline, and power transmission, are considered to be more economical alternatives than the costly stainless steels [16–20]. Unlike the passive metals, e.g., stainless steels and titanium alloys, the carbon steels cannot grow a protective passive film on the surface because of their low content of some alloy elements (Cr, Ni, etc.). For AISI 1045 steel, a porous rust layer with a weak adhesion bond is formed when it is immersed in aggressive electrolytes [21–24]. This oxide layer is not protective, so the corrosive species can easily penetrate through and reach the bare substrate causing continuous corrosion reactions. Although a good understanding of the tribocorrosion behavior of passive metals has been achieved, only a few studies are reported regarding the behavior of active metals. Furthermore, very little is known regarding the tribocorrosion performance differences between passive and active materials.

This study is carried out with an aim of further comprehending the tribocorrosion behavior of AISI 1045 steel and AISI 2205 stainless steel in seawater. A rotatory tribometer equipped with an electrochemical workstation was used for this purpose, which allows an *in-situ* characterization of the surface state of materials during sliding tests. The effect of passive film formation on the tribocorrosion properties was discussed. In addition, the synergy of wear and corrosion was quantified.

2 Experimental procedures

The experiments were performed on AISI 1045 steel and AISI 2205 duplex stainless steel. The chemical compositions and mechanical properties of these two materials are provided in Tables 1 and 2. For the tribocorrosion tests, the specimens were machined into ring shapes each with outer and inner diameters of 54 and 38 mm, respectively. The test surfaces of the specimens were ground down with SiC paper to grade 1,500. Subsequently, they were coated with an epoxy paint, where only the upper surfaces were left exposed to the electrolyte. Afterwards, the specimens were ultrasonically cleaned in acetone followed by rinsing in deionized water, finally, they were dried with air.

The tribocorrosion tests were carried out using a pin-on-disc tribometer integrated with an electrochemical workstation. The schematic of the experimental setup is shown in Fig. 1. The disc samples were used as working electrode (WE) in the experiments and located at the bottom of the electrochemical cell. The reciprocating sliding was achieved by rubbing an inert alumina pin (nominal dimension of Φ 4 mm × 13 mm) against the stationary specimens. The wear tests were conducted under sliding contact at a fixed load of 80 N and a sliding speed of 80 rpm. Both the cell and the specimen holder were made of Teflon, an insulating and corrosion-resistant material, to isolate the specimen from the tribometer. An Ag/AgCl electrode filled with

Table 1 Chemical compositions of AISI 1045 and AISI 2205.

Material	Chemical composition (wt%)						
	Cr	Ni	Mo	C	N	Si	Fe
1045CS	0.15	0.1	—	0.5	—	0.29	Bal.
2205DSS	21.6	5.7	3.3	0.03	0.15	0.4	Bal.

Table 2 Mechanical properties of AISI 1045 and AISI 2205.

Material	Tensile strength (MPa)	Yield strength	Elongation (%)	Density (g/cm^3)	Hardness (Hv)
1045CS	600	335	16	7.85	229
2205DSS	625	450	25.5	7.88	345

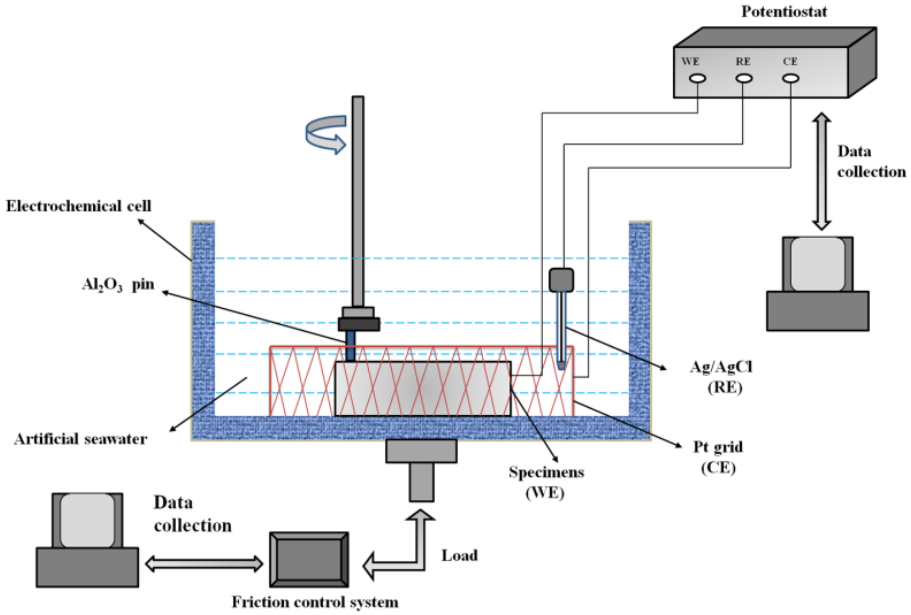

Fig. 1 Schematic of the tribocorrosion tester.

3.5 M KCl was inserted in the cell to serve as the reference electrode (RE). The potential of RE is 205 mV vs. the standard hydrogen electrode, and all the potentials registered in this work are referred to this electrode. A ring of platinum wire was used as the counter electrode (CE) and was positioned at the outer periphery of the electrochemical cell. For all the tribocorrosion tests, the specimens were fully immersed in the artificial seawater, which was prepared according to ASTM D1141 [25]. The PH of the artificial seawater was adjusted to 8.2 by using 0.1 M NaOH solution. Its chemical compositions are provided in Table 3. All the tests were conducted at room temperature (22 ± 2 ℃) and repeated at least three times to verify the reproducibility of the experiments.

For studying the tribocorrosion behavior of AISI 1045 and AISI 2205 steels, several electrochemical methods were employed. Open circuit potential (OCP) measurement was performed under both continuous and intermittent sliding. Under continuous sliding, the OCP curves were monitored as a time function before (20 min), during (60 min), and after (20 min) the sliding. The intermittent sliding tests were carried out with progressively increased normal load and sliding speed, systematically along 20 min with the sliding contact and 20 min without the sliding contact. The test conditions comprised loads of 60, 80, 100, and 120 N at the sliding speed of 80 rpm, and the sliding speeds of 40, 80, 120, and 160 rpm at the load of 80 N. The potentiodynamic polarization measurements, which involved the measurement of polarization curves of the specimens during sliding and without sliding, were performed by changing the potential automatically from –1.2 to +0.8 V at a scanning rate of 2 mV/s.

After the tests, the worn surfaces and wear debris of the specimens were analyzed by scanning electron microscope (SEM, JEOL 5600, Japan). The morphologies of the wear scar on the alumina pin were also examined by SEM equipped with an energy dispersive spectrometer (EDS).

Table 3 Chemical compositions of the artificial seawater.

Compound	NaCl	$MgCl_2$	Na_2SO_4	$CaCl_2$	KCl
Concentration (g/L)	24.530	5.200	4.090	1.160	0.695
Compound	$NaHCO_3$	KBr	$SrCl_2$	H_3BO_3	NaF
Concentration (g/L)	0.201	0.100	0.025	0.027	0.003

3 Results and discussion

3.1 Electrochemical behavior of samples

The OCP measurement is a simple technology that can give valuable information on the surface state

of the worn metal. The OCP measured during tribocorrosion test is a mixed potential that reflects the relative condition between worn and unworn areas. It is reported that this mixed potential primarily depends on factors, such as the kinetics of anodic and cathodic reactions in worn and unworn areas, the ratio and relative position of worn and unworn areas, and the respective intrinsic OCPs of the materials in worn and unworn areas [26]. The variations of OCP with time as a result of sliding wear for AISI 1045 and AISI 2205 are shown in Fig. 2. Before beginning of the sliding, the test samples were immersed in seawater for 1,200 s. A slight increase of the OCP of AISI 2205 was noticed in that time interval. This increase indicates that a stable passive surface state on AISI 2205 is achieved. However, there was a decrease of OCP for AISI 1045 during the initial immersion period, indicating the initiation of corrosion processes in the surface. Once sliding was started, a sudden decrease of the OCP of AISI 2205 was observed, subsequently, this OCP reached a steady state. The cathodic shift is due to the removal or partial removal of the passive film on the alloy surface, then, an equilibrium between the mechanical depassivation and electrochemical repassivation is established. Nevertheless, there is an opposite response for AISI 1045, where the OCP shifted to noble values when sliding was applied. Unlike the case of AISI 2205, an active material, e.g., AISI 1045, does not grow a protective passive film on the surface. The continuous action of alumina pin slowed the corrosion rate in the wear track, as there was a continuous removal of the material in the top of that region [27, 28]. The sliding consequently led to the formation of a macrobattery, where the wear track acts as the cathode and the unworn area acts as the anode. Therefore, the potential in the unworn areas remained more anodic as compared to that of the wear track, and the resultant mixed OCP shifted to an anodic direction. The SEM micrographs in Fig. 3 confirm the different corrosion mechanisms between AISI 1045 and AISI 2205 during the corrosion-wear processes. As observed from Fig. 3(a), corrosion is more severe in the unworn areas of AISI 1045 demonstrating that the sliding

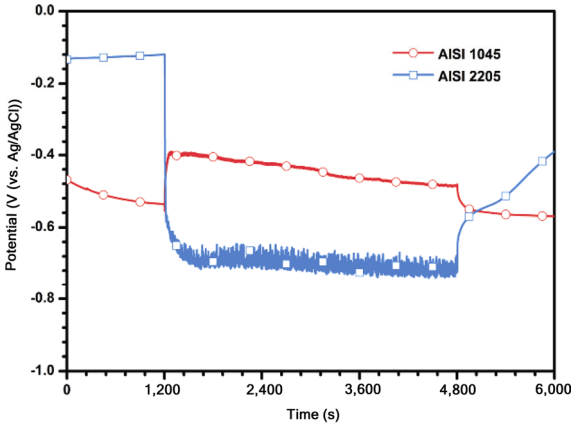

Fig. 2 Evolution of the OCP of tested samples immersed in seawater before, during, and after sliding.

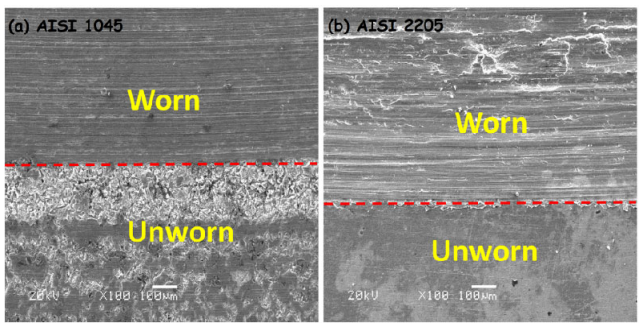

Fig. 3 SEM micrographs of the worn surfaces for (a) AISI 1045 and (b) AISI 2205 after tribocorrosion tests at OCP in seawater.

accelerates the corrosion kinetics outside the wear track. Conversely, for AISI 2205, the corrosion scales are only observed in the worn areas and the unworn surfaces seem to be less prone to corrosion attacks (Fig. 3(b)).

Figure 4 compares the potentiodynamic curves of AISI 1045 and AISI 2205 in the absence and presence of sliding in seawater. When AISI 1045 and AISI 2205 were under static corrosion, the current was stable until the potential reached the localized corrosion potential, –0.2149 V for AISI 1045 and +0.3912 V for AISI 2205 in the anodic region. The electrochemical behavior showed significant differences between the two metals under sliding condition. For AISI 1045 (Fig. 4(a)), the corrosion potential was anodically shifted, suggesting that the corrosion kinetics in the wear track were different from those in the unworn areas, because the sliding contacts hindered the natural trend of corrosion processes and slowed down the corrosion rate in the wear track. Meanwhile, for AISI 2205 (Fig. 4(b)), the corrosion potential was shifted

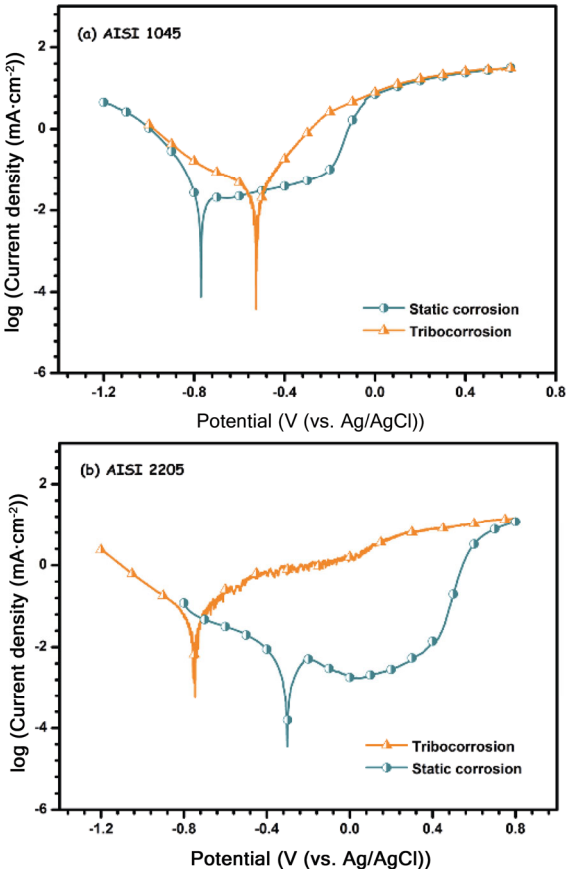

Fig. 4 Potentiodynamic curves of AISI 1045 and AISI 2205 without sliding and under sliding in seawater.

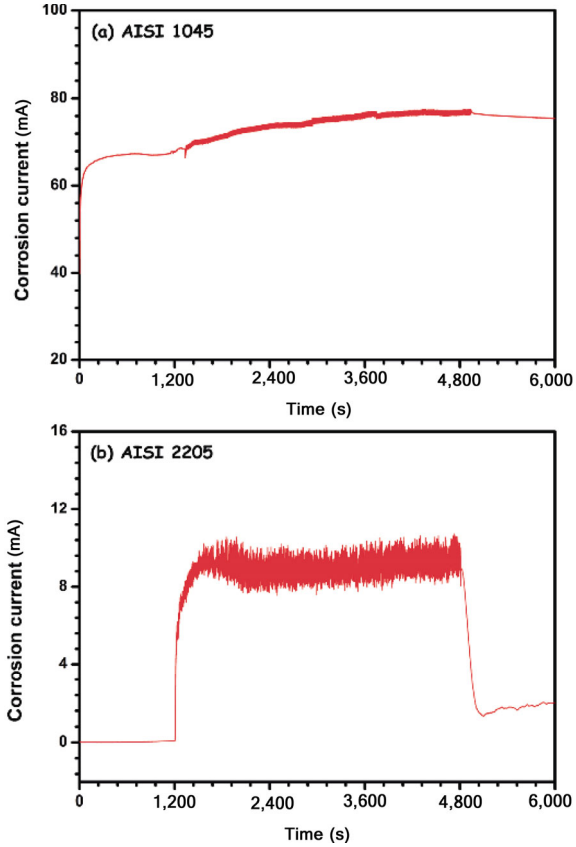

Fig. 5 Evolution of the current recorded before, during, and after sliding at an applied potential of +0.2 V for (a) AISI 1045 and (b) AISI 2205.

cathodically owing to sliding, which is attributed to the destruction of the passive film and the activation of the material in the worn surface. However, the corrosion current densities increased for both AISI 1045 and AISI 2205 under tribo-conditions, indicating that wear increases the corrosion rate of both metals. Under the tribocorrosion condition in Fig. 4(b), some fluctuations were observed because of the active- passive transitions taking place in the worn areas.

The anodic potentiostatic measurements were performed at a constant potential of +0.2 V for both metals, and the results are shown in Fig. 5. Before sliding, the AISI 1045 exhibited a higher current and the current gradually increased to reach values near 70 mA (Fig. 5(a)). Such an increase in the current indicates that AISI 1045 is an active material and undergoes high corrosion rate processes when immersed in seawater. Moreover, the current continued to increase when sliding was applied. However, when AISI 2205 was under a static condition, the current was stable and lower values were observed (Fig. 5(b)). During sliding, a significant increase in current was observed for AISI 2205, because of the removal or damage of the protective oxide film on the contact areas and the accelerated dissolution of the bare metal exposed to seawater. In other words, the corrosion was accelerated by the sliding action, contributing to a wear-accelerated corrosion. When sliding was stopped, the current decreased due to the repassivation of the worn areas.

To study the influence of applied normal load and sliding speed on the OCP during tribocorrosion, the intermittent sliding tests were conducted at various loads (from 60 to 120 N) and speeds (from 40 to 160 rpm), and the results are given in Fig. 6. For AISI 1045, regardless of the load and speed level, the OCP was shifted anodically, when there is a sliding contact, implying that the corrosion susceptibility of AISI 1045 was reduced. Moreover, the smaller the load and speed, the lower the corrosion susceptibility of AISI 1045. As the case of

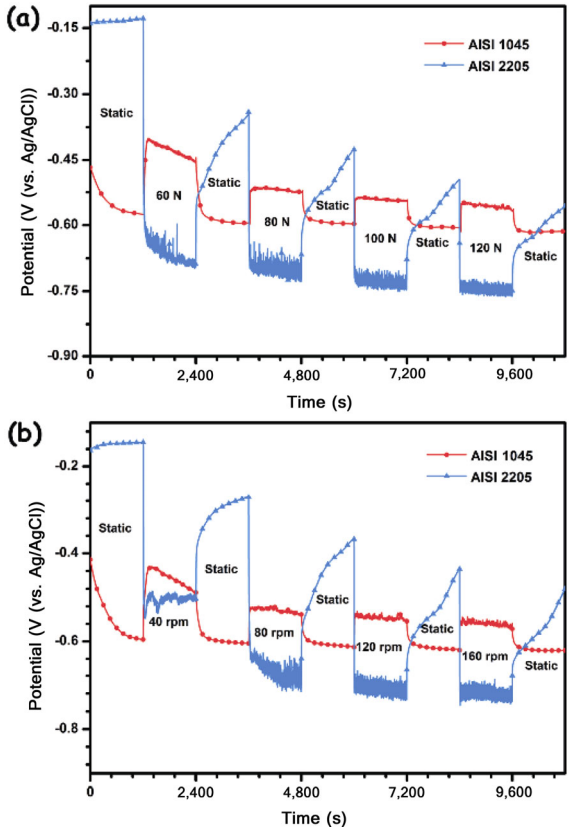

Fig. 6 Evolution of the OCP as a function of time during intermittent sliding under varied (a) load and (b) speed.

AISI 2205, the OCP shifted to the cathodic direction sharply with the onset of sliding and fluctuated around a value associated with the specific load and speed. It was also observed that the degree of the cathodic shift increased with an increase in applied load and sliding speed. The decrease of the OCP with an increased load is due to the increased worn areas for higher load levels, as the OCP is strongly dependent on the ratio of worn and unworn areas. Additionally, the decrease of the OCP with an increase in speed can be explained by the increased contact frequency, therefore, less time is available to allow the metal to repassivate between the two strokes. Figure 7 exhibits the effect of applied potential on the corrosion current of AISI 1045 and AISI 2205 during sliding. It can be observed that by increasing the applied potential, the corrosion rate of metals will be increased to varying degrees, especially for AISI 1045, the corrosion currents of which almost have a larger magnitude than those of AISI 2205 at a specific applied potential. Besides, at the cathodic potential of –0.9 V, the measured currents in both metals were found to be negative, confirming that no electrochemical corrosion occurred on the surface and the total material loss was derived from pure mechanical wear.

3.2 Friction and wear behavior of samples

The coefficient of friction (COF) was measured during sliding tests in seawater, as shown in Fig. 8. The results indicate that the COF of AISI 1045 increased with the sliding time and gradually stabilized. The probable reason is the continuous removal of oxides in contact areas by the counterpart, leading to the modification in size and morphology of the wear track, thereby affecting the contact pressure between the contacting surfaces during sliding. In the case of AISI 2205, the higher COFs are registered

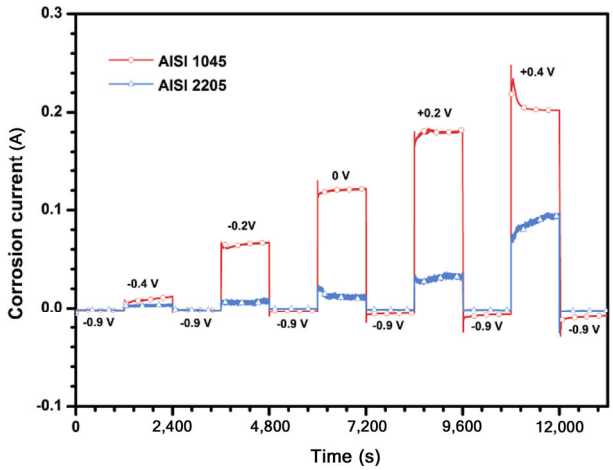

Fig. 7 Effect of applied potential on the corrosion current of AISI 1045 and AISI 2205 during sliding in seawater.

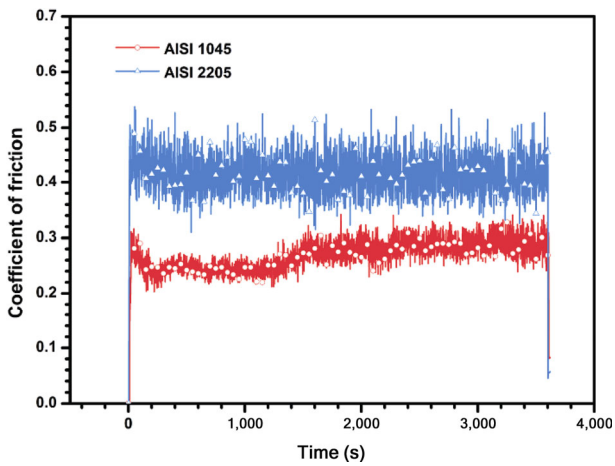

Fig. 8 Dynamic coefficient of friction measured during sliding tests in seawater.

and the fluctuations of the COFs are more pronounced compared with AISI 1045. As discussed above, the passive film of AISI 2205 present on contact areas was removed under sliding action, resulting in an accelerated electrochemical corrosion of the materials inside the wear track. Thus, the increased roughness of the wear track due to the accelerated corrosion made the COFs of AISI 2205 to be higher and fluctuant.

The morphology of worn surface and wear debris for AISI 1045 and AISI 2205 revealed by the SEM is shown in Fig. 9. It is evident that the wear track of AISI 1045 (Fig. 9(a)) is smooth with fine abrasion marks, whereas the wear track of AISI 2205 (Fig. 9(c)) appears to be rough with several deep and wide grooves parallel to the sliding direction, in accordance with the measured average COFs (Fig. 8). Upon combination with the machining chips observed in Figs. 9(b) and 9(d), it demonstrates that the abrasive wear prevailed for both metals during the tribocorrosion processes. The abrasive ploughing effects that occurred on the worn surface after tribocorrosion can be attributed to the harder asperities on alumina counterface that ploughed the softer metal surfaces. This phenomenon is known as two-body abrasion. Meanwhile, for AISI 2205, many residual margins left by the lamellar tearing appeared on the worn surface, and the wear debris constituted a large amount of flaky-like debris. It suggests that delamination was another primary wear mechanism of AISI 2205 during the sliding wear process in seawater. In the case of AISI 1045, the wear debris mainly comprised the flocculent corrosion products, which further confirmed its poor corrosion resistance. To further investigate the wear mechanism of both metals, the SEM morphologies and enlarged views of the alumina counterface were measured, as shown in Fig. 10. Essentially, a nearly complete metal transfer film was formed on the alumina counterface when sliding against AISI 1045 (Figs. 10(a) and 10(a_1)), which transformed the sliding friction between the soft metal and hard ceramic into the metal–metal pairs, greatly reducing the wear rate. Meanwhile, the metallic transfer film was oriented in the direction of sliding, indicating that adhesive wear occurred during the sliding wear process. However, as shown in Figs. 10(b) and 10(b_1), no transfer layer was detected on the alumina counterface sliding against AISI 2205.

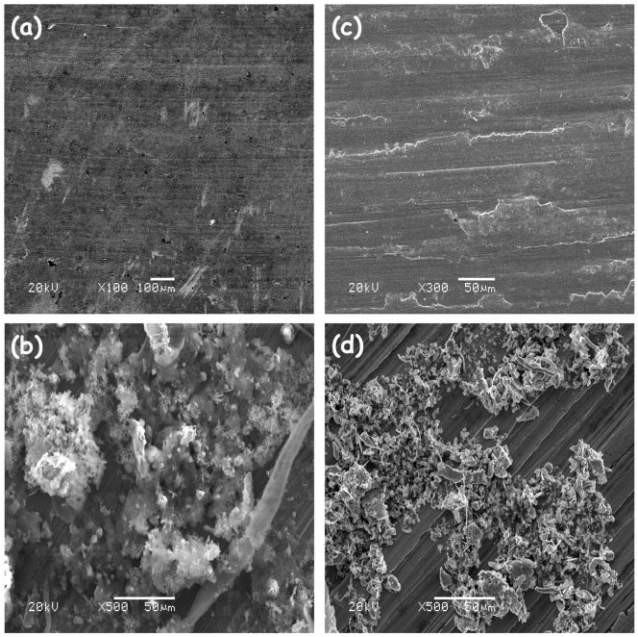

Fig. 9 SEM morphology of worn surface and wear debris for (a, b) AISI 1045 and (c, d) AISI 2205 after tribocorrosion tests.

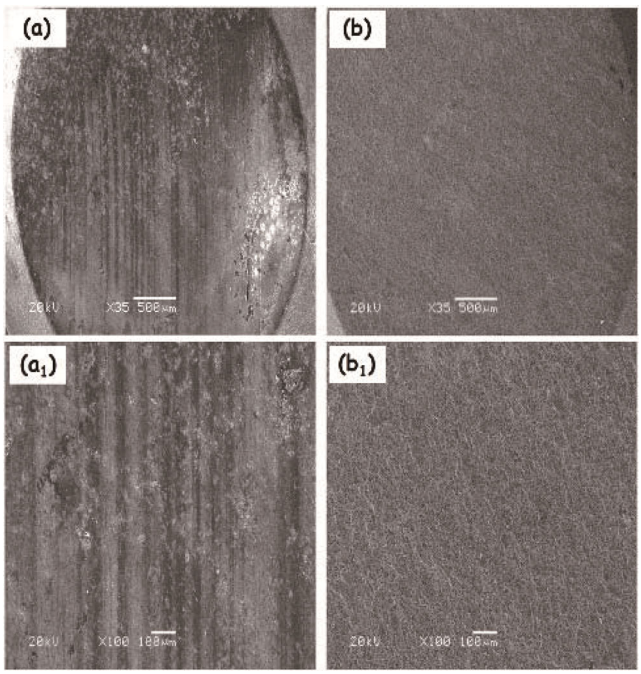

Fig. 10 SEM images and enlarged views showing the morphologies of alumina counterface after sliding against (a, a_1) AISI 1045 and (b, b_1) AISI 2205 steels.

3.3 Wear-corrosion synergism

The measurement of the total mass loss is essential for evaluating the effect of corrosion on the

degradation of metals during sliding wear. Figure 11 shows the total mass loss of AISI 1045 and AISI 2205 due to tribocorrosion process at each potential. The results indicated that in the presence of corrosion, whether at OCP or applied anodic potential, the total mass loss was increased for both metals. Besides, when either the pure mechanical wear (at –0.9 V) or slight corrosion (at OCP) occurred, the total mass loss of AISI 2205 was nearly ten times, as compared to that of AISI 1045, indicating that AISI 1045 showed better tribocorrosion resistance in these conditions. As the applied potential continued to increase, the total mass loss of AISI 1045 sharply increased and it was even larger than that of AISI 2205 at the applied potential of +0.4 V. Based on the presented results, it is clear that the synergism between wear and corrosion for AISI 1045 and AISI 2205 is established. Therefore, the material loss due to tribocorrosion cannot be determined by simply adding the individual contribution due to mechanical wear and corrosion, as the overall material loss somewhat exceeded this sum. The assessment of tribocorrosion behavior was carried out according to the ASTM G119 Standard [29], which allowed the quantification of the contributions of wear and corrosion and their synergism to the material degradation by the calculation of the following parameters. The total material loss (T) comprises three components, including the pure corrosion loss in the absence of wear (C_o), the pure wear loss in the absence of corrosion (W_o), and the material loss due to the synergistic effects between wear and corrosion (S), which is given in Eq. (1):

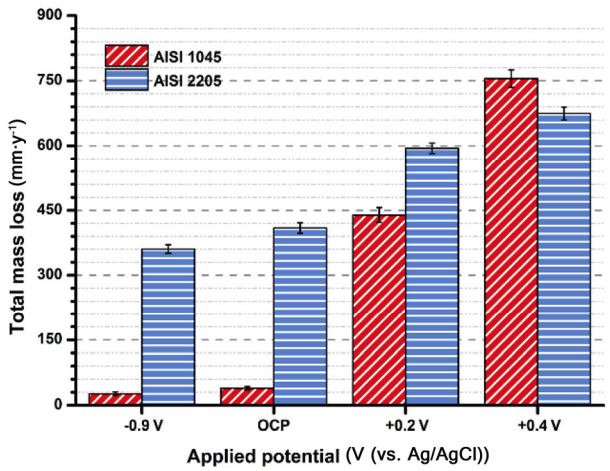

Fig. 11 The total mass loss of AISI 1045 and AISI 2205 at different applied potentials after sliding under 80 N load and 80 rpm speed.

$$T = C_o + W_o + S \quad (1)$$

Furthermore, the synergistic component S can be divided into two components: the increment of corrosion loss due to wear (ΔC_w), and the increment of wear loss due to corrosion (ΔW_c), as shown below:

$$S = \Delta C_w + \Delta W_c \quad (2)$$

Therefore, ΔC_w and ΔW_c can be calculated according to the following equations:

$$\Delta C_w = C - C_o \quad (3)$$

$$\Delta W_c = W - W_o \quad (4)$$

where C denotes the corrosion loss with wear, and W denotes the wear loss with corrosion.

T and W_o can be calculated by the following equations:

$$T = \frac{m_0 - m_1}{S\rho t} \quad (5)$$

$$W_o = \frac{m_0 - m_2}{S\rho t} \quad (6)$$

where m_0 denotes the initial mass of samples, m_1 denotes the final mass of samples after tribocorrosion test, m_2 denotes the final mass of samples after the cathodic protection test, ρ denotes the specimen density, S denotes the area of worn surface, and t denotes the test duration.

According to Faraday's Law, the corrosion rate can be calculated in terms of penetration rate, as follows:

$$C_o = \frac{Mi_o}{ZF\rho} \quad (7)$$

$$C = \frac{Mi_w}{ZF\rho} \quad (8)$$

where M denotes the atomic mass of the alloys, i_o and i_w denote the corrosion current density measured under static corrosion and tribocorrosion conditions, respectively, Z denotes the number of valence electrons involved in the corrosion of the alloy, and F denotes the Faraday's constant (96,500 C/mol).

For describing the degree of synergism between wear and corrosion, three dimensionless factors are defined as follows.

The total synergism factor is

$$\frac{T}{T-S} \quad (9)$$

The wear augmentation factor is

$$\frac{W_o + \Delta W_c}{W_o} \tag{10}$$

The corrosion augmentation factor is

$$\frac{C_o + \Delta C_w}{C_o} \tag{11}$$

The summary of various material loss components for AISI 1045 and AISI 2205 steels at different applied potentials are shown in Tables 4 and 5. The mass fraction of each component in the total material loss of AISI 1045 and AISI 2205 at different applied potentials is shown in Fig. 12. Undoubtedly, when tested under applied cathodic potential (–0.9 V), the material loss is entirely caused by the pure mechanical wear (W_o) for both metals. When measured at OCP, the results showed that the total material loss was primarily caused by pure mechanical wear and corrosion-induced wear (ΔW_c), occupying 67.84% and 30.98% for AISI 1045, and 88.06% and 11.81% for AISI 2205, respectively. However, a significant increase of ΔW_c was noticed with AISI 1045, which attained 62.19% while it was 36.84% for AISI 2205 at +0.2 V. Moreover, the ΔW_c percentage of AISI 1045 was still much bigger than that of AISI 2205 when the applied potential increased to +0.4 V. During the tribocorrosion process at higher anodic potential, the deterioration of the contact surface of the materials by corrosion attack was more severe, which led to the increase in the number of sites for crack nucleation and stress concentration. It has been reported that wear in tribocorrosion is a low cycle fatigue process that involves crack initiation and propagation [30, 31]. Therefore, an active dissolution of both metals at higher anodic potential promoted crack initiation and propagation and resulted in an accelerated wear. At the same time, the wear-induced corrosion was also responsible for the synergism, although its contribution was not predominant at each potential. For AISI 2205, the wear can accelerate corrosion because the sliding action damaged or in some cases removed the passive film, exposing the underlying fresh material to the corrosive electrolyte and consequently leading to accelerated corrosion. As in the case of AISI 1045, unlike passive materials, the material in the wear track possessed a nobler potential than that of the unworn surface when sliding was applied, which suggested that a galvanic couple between worn and unworn surfaces was established, thereby resulting in the wear-accelerated corrosion of the unworn surface. It can also be observed form Fig. 12 that the main source of material loss was different between AISI 1045 and AISI 2205 at +0.2 and +0.4 V. The degradation of AISI 1045 due to tribocorrosion was primarily

Table 4 Summary of various material loss components for AISI 1045 steel at different applied potentials after sliding under 80 N load and 80 rpm speed.

Applied potential (V)	W_0 (mm·y^{-1})	ΔC_w (mm·y^{-1})	C_o (mm·y^{-1})	ΔW_c (mm·y^{-1})	$T/(T–S)$	$(W_0+\Delta W_c)/W_0$	$(C_0+\Delta C_w)/C_0$
–0.9	26.73	—	—	—	—	—	—
OCP	26.73	0.2414	0.2216	12.21	1.462	1.457	2.089
+0.2	26.73	18.10	121.2	273.1	2.969	11.22	1.149
+0.4	26.73	27.20	189.9	511.1	3.485	20.12	1.143

Table 5 Summary of various material loss components for AISI 2205 duplex stainless steel at different applied potentials after sliding under 80 N load and 80 rpm speed.

Applied potential (V)	W_0 (mm·y^{-1})	ΔC_w (mm·y^{-1})	C_o (mm·y^{-1})	ΔW_c (mm·y^{-1})	$T/(T–S)$	$(W_0+\Delta W_c)/W_0$	$(C_0+\Delta C_w)/C_0$
–0.9	360.5	—	—	—	—	—	—
OCP	360.5	0.4995	0.04099	48.36	1.136	1.134	13.18
+0.2	360.5	14.76	0.1362	219.0	1.648	1.607	63.48
+0.4	360.5	11.30	33.60	269.2	1.712	1.747	1.336

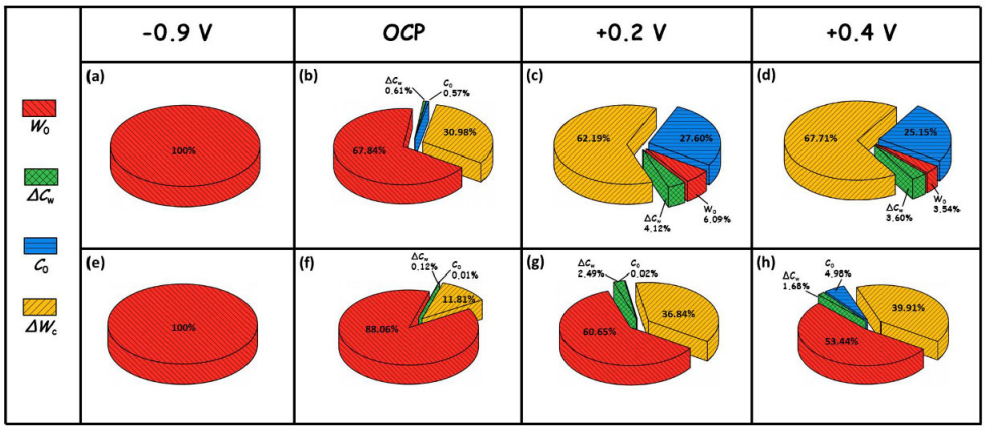

Fig. 12 Contribution of the various degrading components to the total material loss of (a–d) AISI 1045 and (e–h) AISI 2205 at different applied potentials after sliding under 80 N load and 80 rpm speed.

caused by corrosion-induced wear and pure corrosion loss at applied anodic potentials. However, the corrosion-induced wear and pure mechanical wear were dominant in the total material loss of AISI 2205 in the same situation.

4 Conclusions

In the present work, the tribocorrosion behavior of AISI 1045 and AISI 2205 has been investigated in seawater with the aim of comparing the differences between active and passive materials. Therefore, unidirectional tribocorrosion tests were carried out using a pin-on-disc tribometer equipped with an electrochemical workstation. Based on the results obtained, the following conclusions could be drawn:

1) Under the simultaneous action of wear and corrosion, the evolutions of potential of AISI 1045 and AISI 2205 were found to be opposite. For AISI 2205, the OCP shifted cathodically when sliding was applied due to the removal or destruction of the passive film on surface, resulting in the accelerated corrosion in the wear track. However, for the active materials used in this work, such as AISI 1045, an increase in the OCP was observed, which was attributed to the change of the corrosion kinetics of wear track and resulted in the wear-accelerated corrosion in the unworn surface.

2) After tribocorrosion, the wear track of AISI 2205 appeared to be rougher as compared with that of AISI 1045, which was in good agreement with the measured high average COF of AISI 2205. The abrasive and adhesive wear were detected to be the primary wear mechanism for AISI 1045, while the dominant wear mechanism of AISI 2205 was found to be abrasive and delamination wear.

3) The total material loss increased with the increase in applied potential, and there was a clear synergism between wear and corrosion for both metals. However, at applied anodic potentials, the degradation of AISI 2205 was primarily due to pure mechanical wear and corrosion-induced wear, and that of AISI 1045 was due to pure corrosion loss and corrosion-induced wear.

Acknowledgements

The work was financially supported by the National Natural Science Foundation of China (Grant No. 51405478) and Chinese Academy of Sciences "Light of West China" Program.

References

[1] Ben Saada F, Elleuch K, Ponthiaux P. On the tribocorrosion responses of two stainless steels. *Tribol Trans* **61**(1): 53–60 (2018)

[2] García I, Drees D, Celis J P. Corrosion-wear of passivating materials in sliding contacts based on a concept of active wear track area. *Wear* **249**(5–6): 452–460 (2001)

[3] Atık E, Yunker U, Merıç C. The effects of conventional heat treatment and boronizing on abrasive wear and corrosion of SAE 1010, SAE 1040, D2 and 304 steels. *Tribol Int* **36**(3): 155–161 (2003)

[4] Amann T, Gatti F, Oberle N, Kailer A, Rühe J. Galvanically induced potentials to enable minimal tribochemical wear of stainless steel lubricated with sodium chloride and ionic liquid aqueous solution. *Friction* **6**(2): 230–242 (2018)

[5] Dunnwald J, Otto A. An investigation of phase transitions in rust layers using Raman Spectroscopy. *Corros Sci* **29**(9): 1167–1176 (1989)

[6] Bello J O, Wood R J K, Wharton J A. Synergistic effects of micro-abrasion–corrosion of UNS S30403, S31603 and S32760 stainless steels. *Wear* **263**(1–6): 149–159 (2007)

[7] Chen J, Wang J Z, Yan F Y, Zhang Q, Li Q A. Effect of applied potential on the tribocorrosion behaviors of Monel K500 alloy in artificial seawater. *Tribol Int* **81**: 1–8 (2015)

[8] del Abra-Arzola J L, García-Rentería M A, Cruz-Hernández V L, García-Guerra J, Martínez-Landeros V H, Falcón-Franco L A, Curiel-López F F. Study of the effect of sigma phase precipitation on the sliding wear and corrosion behaviour of duplex stainless steel AISI 2205. *Wear* **400–401**: 43–51 (2018)

[9] Diomidis N, Celis J P, Ponthiaux P, Wenger F. A methodology for the assessment of the tribocorrosion of passivating metallic materials. *Lubr Sci* **21**(2): 53–67 (2009)

[10] Huttunen-Saarivirta E, Kilpi L, Hakala T J, Carpen L, Ronkainen H. Tribocorrosion study of martensitic and austenitic stainless steels in 0.01 M NaCl solution. *Tribol Int* **95**: 358–371(2016)

[11] Jun C. Corrosion wear characteristics of TC4, 316 stainless steel, and Monel K500 in artificial seawater. *RSC Adv* **7**(38): 23835–23845 (2017)

[12] Moine M, Mary N, Normand B, Peguet L, Gaugain A, Evin H N. Tribo electrochemical behavior of ferrite and ferrite–martensite stainless steels in chloride and sulfate media. *Wear* **292–293**: 41–48 (2012)

[13] Obadele B A, Andrews A, Shongwe M B, Olubambi P A. Tribocorrosion behaviours of AISI 310 and AISI 316 austenitic stainless steels in 3.5% NaCl solution. *Mater Chem Phys* **171**: 239–246 (2016)

[14] Sun Y, Rana V. Tribocorrosion behaviour of AISI 304 stainless steel in 0.5 M NaCl solution. *Mater Chem Phys* **129**(1–2): 138–147 (2011)

[15] Sun Y W, Yan X P, Yuan C Q, Bai X Q. Insight into tribological problems of green ship and corresponding research progresses. *Friction* **6**(4): 472–483 (2018)

[16] Stratmann M, Bohnenkamp K, Engell H J. An electrochemical study of phase-transitions in rust layers. *Corros Sci* **23**(9): 969–985 (1983)

[17] Stratmann M, Muller J. The mechanism of the oxygen reduction on rust-covered metal substrates. *Corros Sci* **36**(2): 327–359 (1994)

[18] Asami K, Kikuchi M. In-depth distribution of rusts on a plain carbon steel and weathering steels exposed to coastal–industrial atmosphere for 17 years. *Corros Sci* **45**(11): 2671–2688 (2003)

[19] Kamimura T, Hara S, Miyuki H, Yamashita M, Uchida H. Composition and protective ability of rust layer formed on weathering steel exposed to various environments. *Corros Sci* **48**(9): 2799–2812 (2006)

[20] Liu J W, Jiang L, Deng C B, Du W H, Qian L M. Effect of oxide film on nanoscale mechanical removal of pure iron. *Friction* **6**(3): 307–315 (2018)

[21] Guo H X, Lu B T, Luo J L. Interaction of mechanical and electrochemical factors in erosion–corrosion of carbon steel. *Electrochim Acta* **51**(2): 315–323 (2005)

[22] López A, Bayón R, Pagano F, Igartua A, Arredondo A, Arana J L, González J J. Tribocorrosion behaviour of mooring high strength low alloy steels in synthetic seawater. *Wear* **338–339**: 1–10 (2015)

[23] Tamura H. The role of rusts in corrosion and corrosion protection of iron and steel. *Corros Sci* **50**(7): 1872–1883 (2008)

[24] Trausmuth A, Rodríguez Ripoll M, Zehethofer G, Vogl T, Badisch E. Impact of corrosion on sliding wear properties of low-alloyed carbon steel. *Wear* **328–329**: 338–347 (2015)

[25] US-ASTM. ASTM standard D1141-98 Standard practice for the preparation of substitute ocean water. ASTM, 2013.

[26] Tekin K C, Malayoglu U. Assessing the tribocorrosion performance of three different nickel-based superalloys.

Tribol Lett **37**(3): 563–572 (2009)
[27] Cai M R, Yu Q L, Zhou F, Liu W M. Physicochemistry aspects on frictional interfaces. *Friction* **5**(4): 361–382 (2017)
[28] López-Ortega A, Bayón R, Arana J L, Arredondo A, Igartua A. Influence of temperature on the corrosion and tribocorrosion behaviour of High-Strength Low-Alloy steels used in offshore applications. *Tribol Int* **121**: 341–352 (2018)
[29] US-ASTM. ASTM standard G119-09 Standard guide for determining synergism between wear and corrosion. ASTM, 2009.
[30] Zhang B B, Wang J Z, Yan F Y. Load-dependent tribocorrosion behaviour of nickel-aluminium bronze in artificial seawater. *Corros Sci* **131**: 252–263 (2018)
[31] Zhang B B, Wang J Z, Yuan J Y, Yan F Y. Tribocorrosion behavior of nickel aluminum bronze in seawater: Identification of corrosion-wear components and effect of pH. *Mater Corros* **69**(1): 106–114 (2018)

Beibei ZHANG. She received her Ph.D. degree in materialogy from Lanzhou Institute of Chemical Physics, Chinese Academy of Sciences in 2019. She joined the State Key Laboratory of Solid Lubrication at Lanzhou Institute of Chemical Physics from 2019. Her current position is a research assistant. Her research areas cover the metal corrosion and protection.

Fengyuan YAN. He received his M.S. and Ph.D. degrees in tribology and physical chemistry from Lanzhou Institute of Chemical Physics, Chinese Academy of Sciences, in 1991 and 1997, respectively. He joined the State Key Laboratory of Solid Lubrication at Lanzhou Institute of Chemical Physics from 1999. His current position is a professor. His research areas cover the ocean tribology, tribological mechanism of composites, functional materials, and tribological testing technique.